Arch. Metall. Mater. **65** (2020), 2, 923-933

DOI: 10.24425/amm.2020.132840

J. MIETTINEN[1], V.-V. VISURI[1*], T. FABRITIUS[1], G. VASSILEV[2]

THERMODYNAMIC DESCRIPTION OF TERNARY Fe-B-X SYSTEMS. PART 7: Fe-B-C

Thermodynamic description of the Fe-B-C system in its iron-rich corner is developed in the context of a new Fe-B-X (X = Cr, Ni, Mn, Si, Ti, V, C) database. The thermodynamic parameters of the binary sub-systems, Fe-B, Fe-C and B-C, are taken from earlier assessments modifying the B-C description. The parameters of the Fe-B-C system are optimized in this study using experimental thermodynamic and phase equilibrium data from the literature. Liquid, beta-rhombo-B and graphite phases are described using the substitutional solution model, while the ferrite (bcc), the austenite (fcc), the cementite (M_3C) and the $M_{23}C_6$ phases are described with the sublattice model and the borides, Fe_2B, FeB and B_4C, are treated as stoichiometric phases. A good correlation was obtained between the calculated and the experimental thermodynamic and phase equilibrium data. The description is recommended to be used at the composition region of wt% C + wt% B < 15 and at temperatures below 2700ºC.

Keywords: phase diagrams, thermodynamic modelling, thermodynamic database, Fe-B-X systems, Fe-B-C system

1. Introduction

The current contribution builds upon our earlier started research [1] on a boron containing iron-based Fe-B-X database, where boron is treated as a substitutional component. To this end, a few pertinent descriptions have been published earlier [1-6] using the ThermoCalc software [7].

Moreover, a general Iron Alloys Database (IAD) is under development [8]. This database adapts the format of the ThermoCalc databases comprising the following components: Fe, Al, B, C, Ca, Ce, Cr, Cu, H, Mg, Mn, Mo, N, Nb, Ni, O, P, S, Si, Ti and V. IAD is be applied in an Inter Dendritic Solidification (IDS) solidification model [9, 10] used to simulate the non-equilibrium solidification of steels as well as their solid-state phase transformations, including precipitate formation or dissolution, depending on the cooling/heating history. As IDS simulates non-equilibrium solidification (taking kinetics into account), the calculation times are longer than in conventional thermodynamic software simulating equilibrium solidification. This becomes a problem in the real-time online processes of continuous casting, where numerous strand intersections need to be simulated at the same time [11]. For this reason, few simplifications [8] were made to some phase descriptions of the IAD database to reduce the computation times. These simplifications cause typically very slight or ignorable deviation in the calculated results. Consequently, there is no fitting problem if one wants to apply the earlier assessed (not-simplified) data in the calculations.

A thermodynamic optimization of the Fe-B-C system was performed using the ThermoCalc software [7] and experimental thermodynamic and phase equilibrium data from the literature. The new description is focused on the iron-rich corner of the system. The system has been assessed by Hasebe et al. [12], Nishizawa et al. [13] and Ohtani et al. [14], but these descriptions could not be used directly since their binary Fe-B and Fe-C data differ from those of the current Fe-B-X database. A thermodynamic Fe-B-C description is also available in the ThermoCalc software [7] (database TCFe7) but this description has not been shown in the open literature. Another reason for deriving a new description is that the earlier studies treated B as an interstitial component in most solution phases, whereas the current database, including the earlier Fe-B-X descriptions [1-6], treats it as a substitutional component in all solution phases. This is a practical choice made in our first Fe-B-X description [1] based on the binary Fe-B assessment of Hallemans et al. [15]. The binary thermodynamic data used in the current Fe-B-C description is taken from Miettinen and Vassilev [1] for the Fe-B system, from Gustafson [16] for the Fe-C system and from Kasper and Lukas [17] for the B-C system. The models of

[1] "UNIVERSITY OF OULU, PROCESS METALLURGY RESEARCH UNIT, P.O. BOX 4300, 90014 UNIVERSITY OF OULU, FINLAND
[2] UNIVERSITY OF PLOVDIV, FACULTY OF CHEMISTRY, 24 TSAR ASEN STR., 4000 PLOVDIV, BULGARIA

* Corresponding author: ville-valtteri.visuri@oulu.fi

the beta-rhombo-Band B_4C phases used by [17] were changed in this study, treating beta-rhombo-B as a substitutional solution phase and B_4C as a simple stoichiometric phase. These treatments simplify the calculations of the IDS software and only marginally affect the calculated phase equilibria in the iron-rich part of the Fe-B-C system. Note also the unusual choice in the present Fe-B-C description to treat B as a substitutional component in the bcc and fcc phases but C as an interstitial one [16]. This is intended to simplify the use of the present Fe-B-C description. But we also present an alternative Fe-B-C description treating both B and C as substitutional components; this description is applied in the IDS software.

2. Phases, modeling and data

Table 1 shows the phases and their modeling in the current Fe-B-C assessment. The liquid, beta-rhombo-B and graphite phases are described with a substitutional solution model, while the bcc (base centered cubic phase or ferrite), fcc (face centered cubic phase or austenite), the M_3C (cementite) and $M_{23}C_6$ phases are described with sublattice models and the borides, Fe_2B, FeB and B_4C, are treated as stoichiometric phases. Detailed descriptions of the substitutional solution and sublattice models and their parameters are available from Andersson [18]. This work introduces the phase descriptions of the Fe-Cr-C system but by replacing Cr with B, they can be applied to the phases of the current Fe-B-C system.

Experimental studies for the Fe-B and Fe-C systems have been reviewed by Miettinen and Vassilev [1] and Gustafson [16], respectively. The experimental phase equilibrium data applied in these optimizations are from [19-24] for the Fe-B system and from [25-32] for the Fe-C system. For the B-C system, experimental phase equilibrium data of [33-35] was used to achieve simpler descriptions for the beta-rhombo-B (bet) and B_4C phases than those in the optimization by Kasper and Lukas [17].

Experimental studies of the Fe-B-C system have been reviewed earlier by Raghavan [36] (before 1992) and Rogl [37] (before 2008). However, there are also some more recent measurements available. Table 2 shows the experimental information [38-52] selected for the current optimization of the Fe-B-C system.

TABLE 1

Phases and their modeling in the current Fe-B-C description

Phase	Modeling
liquid (L)	(B,C,Fe), substitutional, RKM[a]
bcc_A2 (bcc, ferrite, α-Fe)	(B,Fe:C,Va), sublattice, RKM
fcc_A1 (fcc, austenite, γ-Fe)	(B,Fe:C,Va), sublattice, RKM
beta-rhombo-B (bet)	(B,C), substitutional, RKM
graphite (gra)	(B,C), substitutional, RKM
M_3C (cementite, dissolving B)	$(Fe)_3(B,C)$, sublattice, RKM
$M_{23}C_6$ (dissolving B)	$(Fe)_{23}(B,C)_6$, sublattice, RKM
Fe_2B	$(Fe)_2(B)$, stoichiometric
FeB	(Fe)(B), stoichiometric
B_4C	$(B)_9(C)_2$, stoichiometric

[a] RKM = Redlich-Kister-Muggianu (Gibbs excess energy model)

3. Results

The thermodynamic description of the Fe-B-C system is presented in Table 3. The parameters marked with a reference code were adopted from earlier assessments [1,15-17,53-55] and those marked with O* were optimized using the Calphad approach [56]. This is a semi-empirical method for modeling thermodynamic properties of multicomponent alloys using all experimental and theoretical information available on the phase equilibria and the thermochemical properties of the system. The experimental data employed in the current optimization is summarized in Table 2. Note the strong temperature and composition dependency of the ternary liquid-state interaction parameter of $L^{L}_{B,C,Fe}$, which was necessary to achieve a reasonable accordance between the calculations and the measurements at any temperature. Also note the alternative data for the $M_{23}C_6$ phase. With this parameter expression, the temperature making $M_{23}C_6$ unstable could be increased from 390°C to 500°C, which agrees better with the suggestions of [36,37] that $M_{23}C_6$ could decompose slightly below 600°C. This subject is discussed more closely later in the text. Finally, note the Gibbs energy expression of Gustafson [16] for the Fe-C cementite, Fe_3C, applying H_{SER} [53] as a reference state for the components (i.e. the enthalpy of the pure component in its reference phase at 298.15 K). This function has later been re-optimized by Hallstedt et al. [57], but it could not be adopted in the current study as the whole IAD database is based strongly upon the use of the function of Gustafson [16]. Nevertheless, at high temperatures (T > 1000 K), the function of Hallstedt et al. [57] was reported to agree well with that of Gustafson [16].

TABLE 2

Experimental data applied in the optimization of the Fe-B-C system

Experimental data	Reference
Primary precipitation surfaces and liquidus isotherms	[38-40]
Activity of Fe in liquid at 1600°C along composition line $x_C = 0.17 - 0.35x_B$	[41]
Activity coefficient f_C^B in liquid Fe-B-0.22wt%C alloys at 1600°C	[42]
Activity coefficient f_C^B in liquid Fe-1wt%B-C alloys at 1455°C and 1360°C	[43]
Graphite solubility in liquid with Fe isoactivity lines at 1600°C	[41,44,45]
Graphite solubility in liquid phase at 1600 to 1300°C	[44,46,47]
3 vertical sections at 0.5 wt% C, 0.7 wt% and 2.6 wt% B	[39,40,48,49]
7 isothermal sections at 1200°C, 1000°C, 950°C, 900°C, 850°C, 800°C and 700°C	[38,40,50-52]

TABLE 3

Thermodynamic description of the Fe-B-C system. The thermodynamic data of pure components was taken from [53] unless not shown in the table. Parameter values except for T_C and β are in J/mol. T_C and β are the Curie temperature (K) and the effective magnetic moment (magneton) of a phase, respectively

liquid (1 sublattice, sites: 1, constituents: B,C,Fe)	**Ref.**
$L^{L}_{B,Fe} = -133438 + 33.946T + 7771(x_B - x_{Fe}) + 29739(x_B - x_{Fe})^2$	[15]
$L^{L}_{B,C} = -67045 + 4.47T + (-36683 + 2.446T)(x_B - x_C)$	[17]
$L^{L}_{C,Fe} = -124320 + 28.5T + 19300(x_C - x_{Fe}) + (49260 - 19T)(x_C - x_{Fe})^2$	[16]
$L^{L}_{B,C,Fe} = (140000 + 50T)x_B + (140000 + 50T)x_C + (-340000 + 250T)x_{Fe}$	O*
bcc (2 sublattices, sites: 1:3, constituents: B,Fe:C,Va)	
${}^{o}G^{bcc}_{Fe:Va} = {}^{o}G^{bcc}_{Fe}$	[53]
${}^{o}G^{bcc}_{B:Va} = {}^{o}G^{bet}_{B} + 43514 - 12.217T$	[54]
${}^{o}G^{bcc}_{Fe:C} = {}^{o}G^{bcc}_{Fe} + 3{}^{o}G^{gra}_{C} + 322050 + 75.667T$	[16]
${}^{o}G^{bcc}_{B:C} = {}^{o}G^{bet}_{B} + 3{}^{o}G^{gra}_{C} + 200000$	O*
$L^{bcc}_{B,Fe:Va} = -50000 + 42T$	[1]
$L^{bcc}_{Fe:C,Va} = -190T$	[16]
$Tc^{bcc} = 1043y_{Fe}$	[16]
$b^{bcc} = 2.22y_{Fe}$	[16]
fcc (2 sublattices, sites: 1:1, constituents: B,Fe:C,Va)	
${}^{o}G^{fcc}_{Fe:Va} = {}^{o}G^{fcc}_{Fe}$	[53]
${}^{o}G^{fcc}_{B:Va} = {}^{o}G^{bet}_{B} + 50208 - 13.478T$	[54]
${}^{o}G^{fcc}_{Fe:C} = {}^{o}G^{fcc}_{Fe} + {}^{o}G^{gra}_{C} + 77207 - 15.877T$	[16]
${}^{o}G^{fcc}_{B:C} = {}^{o}G^{bet}_{B} + {}^{o}G^{gra}_{C} + 155000$	O*
$L^{fcc}_{B,Fe:Va} = -66000 + 50T$	[1]
$L^{fcc}_{Fe:C,Va} = -34671$	[16]
$Tc^{fcc} = -201y_{Fe}$	[16]
$b^{fcc} = -2.1y_{Fe}$	[16]
beta–rhombo–B (1 sublattice, sites: 1, constituents: B,C)	
${}^{o}G^{bet}_{C} = {}^{o}G^{gra}_{C} + (10000)$	O*
$L^{bet}_{B,C} = (10000)$	O*
graphite (1 sublattice, sites: 1, constituents: B,C)	
${}^{o}G^{gra}_{B} = {}^{o}G^{bet}_{B} + 5000$	[17]
$L^{gra}_{B,C} = 34386 + 8.679T$	[17]
M_3C (2 sublattices, sites: 3:1, constituents: Fe:B,C)	
${}^{o}G^{M3C}_{Fe:B} = 3{}^{o}G^{bcc}_{Fe} + {}^{o}G^{bet}_{B} - 79000 + 12T$	O*
${}^{o}G^{M3C}_{Fe:C} = 3H^{SER}_{Fe} + H^{SER}_{C} - 10745 + 706.04T - 120.6TlnT$	[16]
$L^{M3C}_{Fe:B:C} = 7700 - 4T$	O*
$M_{23}C_6$ (3 sublattices, sites: 20:3:6, constituents: Fe:Fe:B,C)	
${}^{o}G^{M23C6}_{Fe:Fe:B} = 23{}^{o}G^{bcc}_{Fe} + 6{}^{o}G^{bet}_{B} - 435000 + 60T$	O*
${}^{o}G^{M23C6}_{Fe:Fe:B} = 23{}^{o}G^{bcc}_{Fe} + 6{}^{o}G^{bet}_{B} - 291500 - 996T + 132TlnT$	O**
${}^{o}G^{M23C6}_{Fe:Fe:C} = 23/3{}^{o}G^{M3C}_{Fe:C} + (6 - 23/3){}^{o}G^{gra}_{C} + 15000$	[55]
$L^{M23C6}_{Fe:Fe:B:C} = -204000 + 110T$	O*
Fe_2B (2 sublattices, sites: 2:1, constituents: Fe:B)	
${}^{o}G^{Fe2B}_{Fe:B} = 2{}^{o}G^{bcc}_{Fe} + {}^{o}G^{bet}_{B} - 78783 + 10.398T$	[15]
FeB (2 sublattices, sites: 1:1, constituents: Fe:B)	
${}^{o}G^{FeB}_{Fe:B} = {}^{o}G^{bcc}_{Fe} + {}^{o}G^{bet}_{B} - 70300 + 12T$	[1]
B_4C (2 sublattices, sites: 9:2, constituents: B:C)	
${}^{o}G^{B4C}_{B:C} = 9{}^{o}G^{bet}_{B} + 2G^{gra}_{C} - 268000 + 20T$	O*

O* – Parameter optimized in this work

O** – Alternative data making the $M_{23}C_6$ phase to disappear at 500°C

The calculated results were compared to the respective original experimental data to verify the optimization. All calculations were carried out with the ThermoCalc software [7].

Figures 1 and 2 show the Fe-B and Fe-C phase diagrams calculated using the parameters of [1] and [16], correspondingly. The agreement with the experimental data [19-32] is good. The calculated B-C phase diagram is presented in Figure 3. The composition range of the B_4C phase calculated by Kasper and Lukas [17] is wider than that assessed in the current study and their results agree better with the measurements. But as already mentioned, a simplified B_4C phase description has been used in this work.

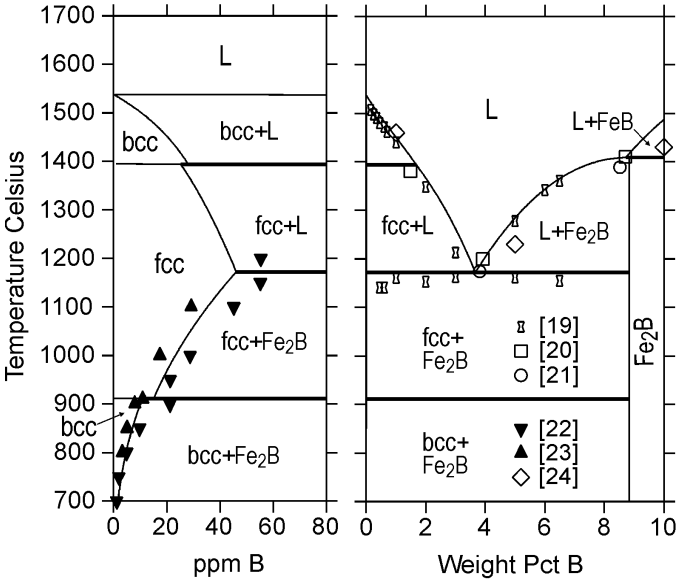

Fig. 1. Fe-B phase diagram calculated by Miettinen and Vassilev [1], together with experimental data points [19-24]

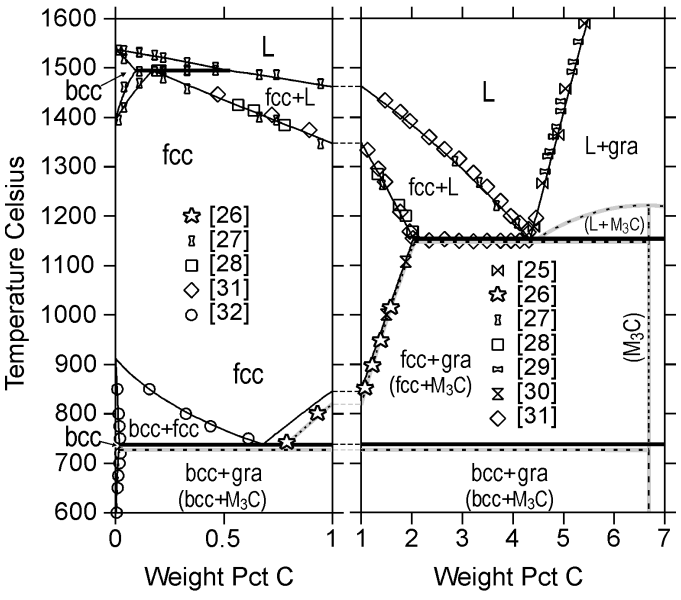

Fig. 2. Fe-C phase diagram calculated by Gustafson [16]together with experimental data points [25-32]. Dotted lines refer to calculations after suspending the graphite phase

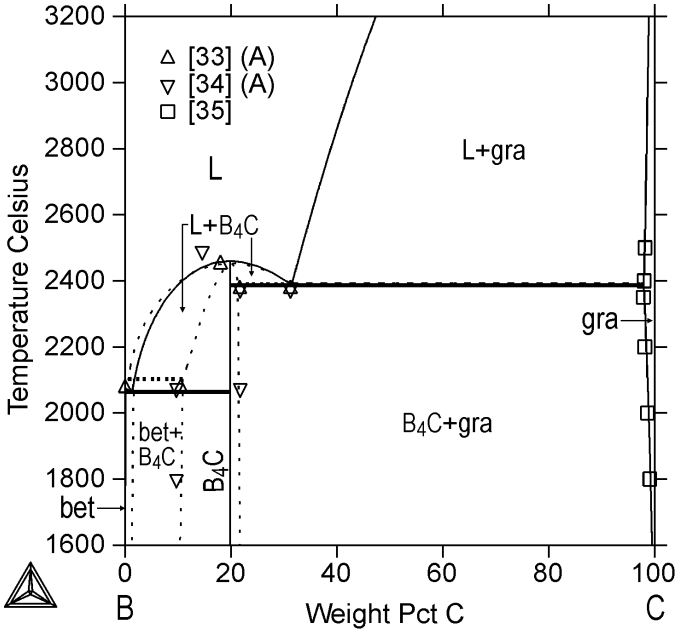

Fig. 3. Calculated B-C phase diagram, together with experimental data points [33-35].The letter A denotes the assessed data. Solid lines refer to the current calculations and the dotted lines refer to those by Kasper and Lukas [17]

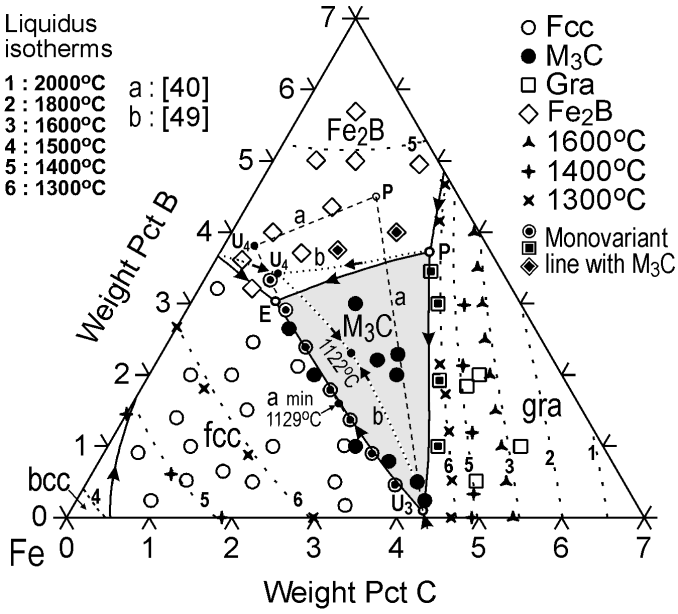

Fig. 4. A calculated liquidus projection of the Fe-B-C system, together with experimental data by Kaneko et al. [38] and Borlera and Pradelli [39], and those assessed by Schürmann and Li [40]. Shown also are the calculated liquidus isotherms between 2000°C and 1300°C (dotted lines), together with experimental data points by Huang et al. [47] and those assessed by Schürmann and Li [40]. The lines suggested by [40] and calculated by Lentz et al. [49] are shown by the letters 'a' and 'b'

Figures 4 to 20 show the results of calculations for the Fe-B-C system, together with the experimental data (Table 2). The agreement is good. Concerning the calculated liquidus projection of Figure 4, note that there is no general agreement between the experimental results of various studies, as stated also by Raghavan [37]. In calculations, no primary precipitation surface of $M_{23}C_6$ was formed, which has been confirmed by seven studies [14,38,40,50,51,60,61], although two contrary views have also been presented [62,63]. The presence of the primary precipitation surface of M_3C, instead, has widely been accepted. In Figure 4, the calculated M_3C surface is shown in grey. This fits well with the experimental primary surface determinations by Kaneko et al. [38] and Borlera and Pradelli [39], including the fcc/L/M_3C monovariant line suggested by Schürmann and Li [40] and the M_3C/L/gra monovariant line estimated from the measurements of [38, 39] and the suggestion of [40]. Both of these lines are shown by the open symbols with black dots inside. In the latter case, the selected M_3C/L/gra line (symbols) represents a compromise made from the studies by [38-40]. The

TABLE 4

Calculated (calc.) and experimental (exp.) invariant points in the Fe-B-C system

Reaction	Type	*t* (°C)	wt % B in L	wt % C in L	Reference
L + B_4C = FeB + gra	U_1	1565	12.41	0.89	Calc this study
L + FeB = Fe_2B + gra	U_2	1357	7.61	1.36	Calc this study
		1350	7.2	0.7	Exp [40]
L + Fe_2B + gra = M_3C	P	1216	3.74	2.54	Calc this study
		1191	4.5	1.5	Exp [40]
L + gra = fcc + M_3C	U_3	1149	0.07	4.29	Calc this study
		1145	0.2	4.10	Exp [40]
L = Fe_2B + fcc + M_3C	E	1137	3.03	1.01	Calc this study
	E	1097	3.24	1.25	Exp [36]
L + Fe_2B = fcc + M_3C	U_4	1132	3.42	0.85	Calc [49]
	U_4	1148	3.7	0.5	Exp [40]
	U_4	1100	2.8	1.0	Exp [38]

calculated M_3C surface, however, does not extend to such high B compositions as indicated by some experimental data points close to 4 wt% B and the invariant point P suggested by [40]. On the other hand, one may question the reliability of the latter point, since the broken line connecting invariant points of U_3 and P of [40] splits the experimental M_3C region of Figure 4, making it possibly too narrow.

Figure 4 also shows the fcc/L/M_3C and M_3C/L/gra monovariant lines calculated by Lentz et al. [49] using the ThermoCalc software with the TCFe7 database (see the dense dotted lines). In their fcc/L/M_3C line, a temperature minimum of 1122°C was obtained, which agrees well with the minimum of 1129°C suggested by Schürmann and Li [40]. The compositions of those minima, however, are quite different, whereas the point of [40] is almost located in the fcc/L/M_3C line of the present calculation. On the other hand, the corresponding temperature close to that composition is a bit higher (1144°C) indicating somewhat lower stability for the liquid phase than suggested by [40]. It was difficult to increase the stability (by calculations) without losing the good accordance obtained between the calculated and experimental M_3C surface. A good indication of that may be the overly narrow M_3C surface calculated by Lentz et al. [49] using data from a more stable liquid phase description.

The numerical data of the invariant points in Figure 4 are given in Table 4. Note that the calculated compositions of these points are somewhat different from those suggested by Schürmann and Li [40]. In addition, the reaction L + Fe_2B = fcc + M_3C (U_4) was proposed by [40] conflicting with the calculated eutectic reaction of L = Fe_2B + fcc + M_3C (E). The reason for the transition reaction (U_4) is the earlier discussed temperature minimum of 1129°C on the monovariant line of fcc/L/M_3C (see Figure 4), whereas according to calculations, the temperature decreased continuously from U_3 (1149°C) to E (1137°C). Note, however, the large scatter in the calculated and suggested composition and temperature values of invariant point E/U_4, which leaves an accurate determination of the corresponding reaction and its location in Figure 4 uncertain. An additional calculation was carried out for the reaction L + B_4C = FeB + gra (U_1) (not shown in Figure 4) using the more complex B_4C description of Kasper and Lukas [17]. This resulted in temperature and composition values of 1567°C, 12.51 wt% B and 0.88 wt% C for the invariant point U_1 which agree well the values given in Table 4. Consequently, treating B_4C as a stoichiometric phase can be considered a reasonable simplification in the present iron-rich description of the system.

Figures 5 and 6 illustrate the calculated Henrian activity data of the liquid phase. The agreement with measurements by Miki et al. [41], Burlyev [42] and Ball [43] is reasonable when taking

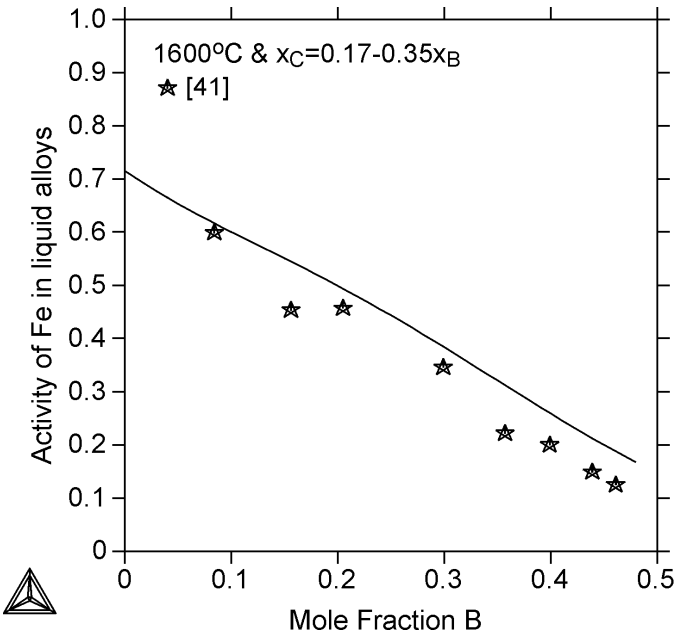

Fig. 5. Calculated activity of Fe in liquid Fe-B-C alloys at 1600°C along the composition line $x_C = 0.17 - 0.35x_B$, together with experimental data points by Miki et al. [41]. The graphite phase was suspended from the calculations. The reference state used is pure liquid Fe

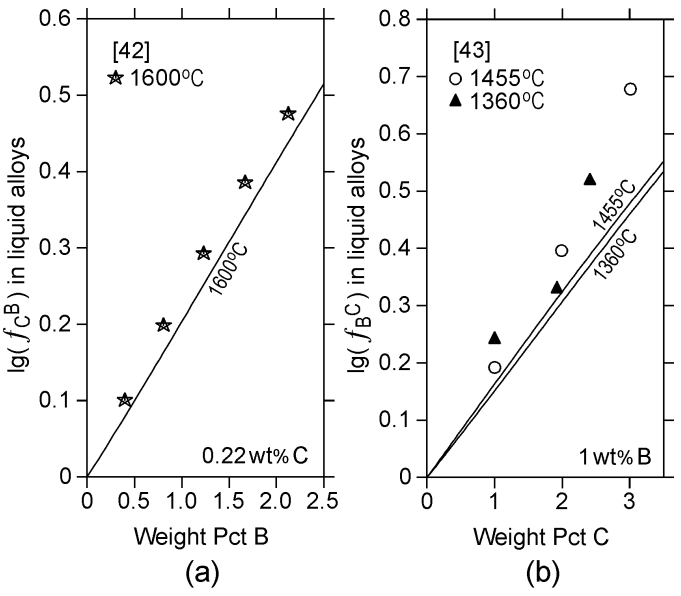

Fig. 6. Calculated Henrian activity coefficients of f_C^B (a) and f_B^C (b) in liquid Fe-B-C alloys, together with experimental data points by Burlyev [42] and Ball [43]

into account that the corresponding measurements indicate relatively low liquid phase stability at high temperatures, in regard to the high stability at low temperatures according to Schürmann and Li [40]. This, in fact, is the reason it was necessary to use the earlier stated strong temperature dependency for the ternary liquid–state interaction parameter of $L^{L}_{B,C,Fe}$. According to that choice, the increasing temperature did not stabilize the liquid phase too much and the agreement, particularly for the B and C activity coefficients (Figure 6), remained reasonable. Additional thermodynamic data is available from Witusiewicz [64] for the enthalpy of mixing of liquid Fe-B-C alloys at 1627°C. Increasing the carbon composition makes this enthalpy data more negative, but not so much as predicted by the calculations.

Figures 7 and 8 show the calculated graphite solubilities in the liquid phase at 1600°C up to 11.4 wt% B (x_B = 0.40) and at 1600°C to 1300°C up to 3 wt% B, respectively. The agreement with measurements by Schenck et al. [44], Sunkar and Morita [45], Miki et al. [41], Yu et al. [46] and Huang et al. [47] is relatively good indicating reasonable stability for the liquid phase at high temperatures. In the latter case, also shown are some iron isoactivity lines in the liquid. The agreement with the measurements by [45] is reasonable. Sunkar and Morita [45] also measured the B activities in liquid, but these data do not agree so well with the calculations. This is mainly due to the higher B activities in binary Fe-B alloys by [45] in regard to the calculated activity values and those measured by Yukinobu et al. [58] and Zaitsev et al. [59].

Figures 9 through 11 show calculated vertical sections of the system at 0.5 wt% C, 0.7 wt% C and 2.6 wt% B, respectively. The agreement with the experimental data of Vogel and Tammann [48], Borlera and Pradelli [39], Schürmann and Li [40]

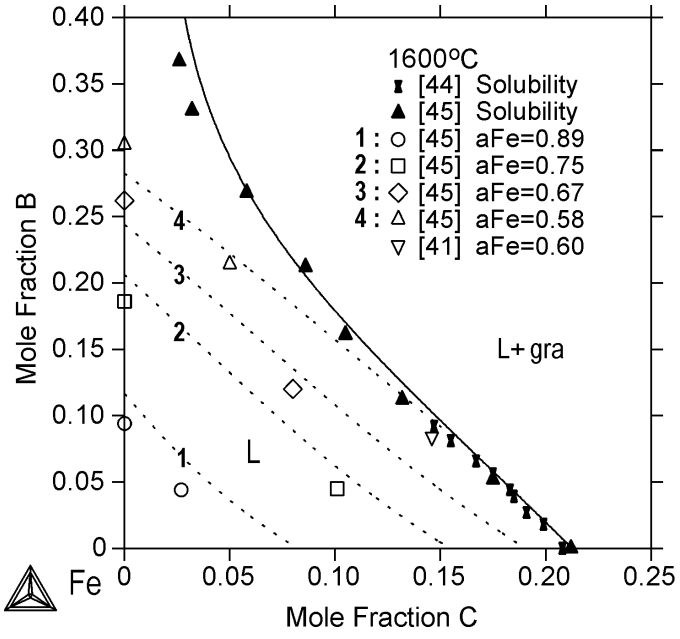

Fig. 7. Calculated graphite solubility in the liquid phase of the Fe-B-C system at 1600°C, together with experimental data points by Schenck et al. [44], Sunkar and Morita [45] and Miki et al. [41]. Shown also are some iron isoactivity lines for the liquid phase (dotted lines). The reference state used is pure liquid Fe

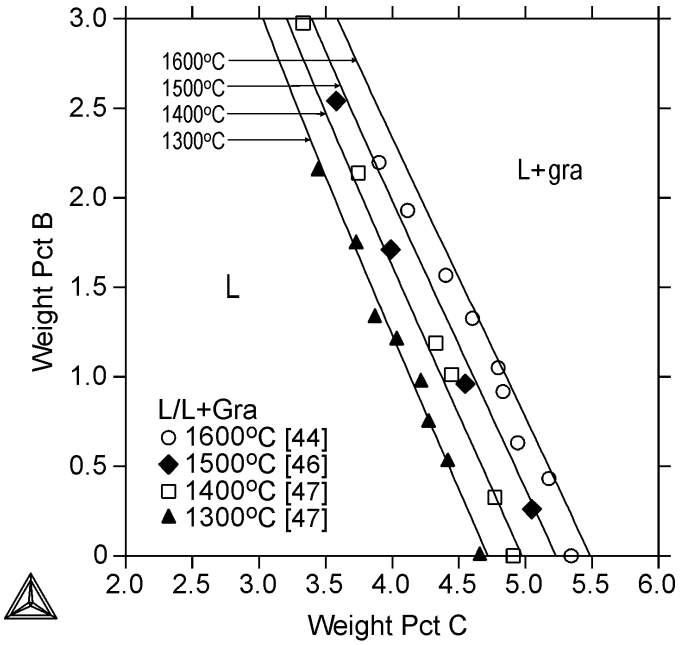

Fig. 8. Calculated graphite solubility in the liquid phase of the Fe-B-C system at 1600°Cto 1300°C, together with experimental data points by Schenck et al. [44], Yu et al. [46] and Huang et al. [47]

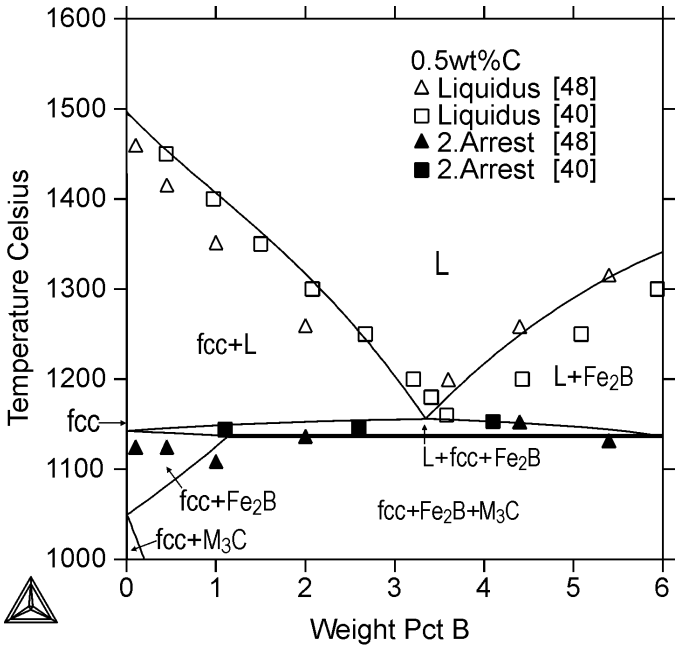

Fig. 9. Calculated vertical section of the Fe-B-C system at 0.5wt%C, together with experimental data points by Vogel and Tammann [48] and Schürmann and Li [40]. The data from [40] is estimated

and Lentz et al. [49] can be considered reasonable. In Figure 11, note the wider L + gra region by [40] pushing the temperature of M_3C formation from the calculated value of 1219°C down to 1180°C. More vertical sections are available from [48] but due to the absence of reliable measurements for determining the phase equilibria with M_3C and $M_{23}C_6$, these sections are not considered here.

Figures 12 to 18 show seven calculated isothermal sections for the system at 1200°C, 1000°C, 950°C, 900°C, 850°C, 800°C

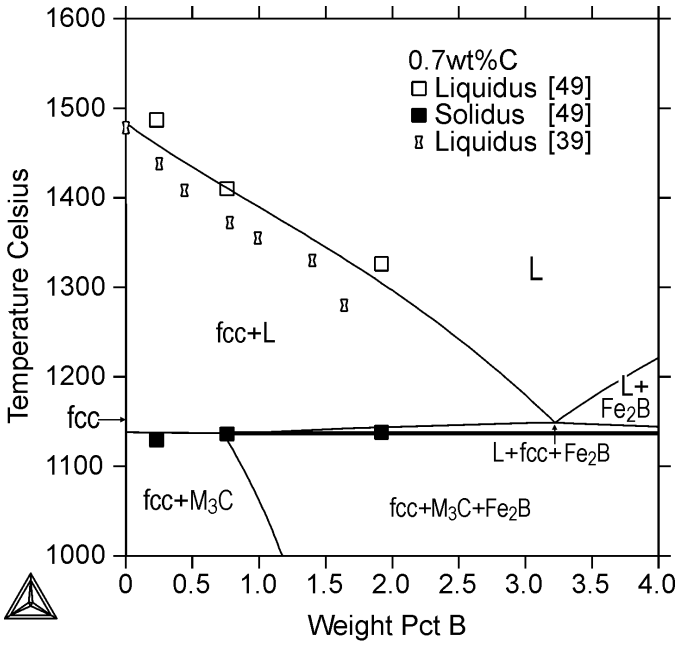

Fig. 10. Calculated vertical section of the Fe-B-C system at 0.7wt%C, together with experimental data points of Borlera and Pradelli [39] and Lentz et al. [49]

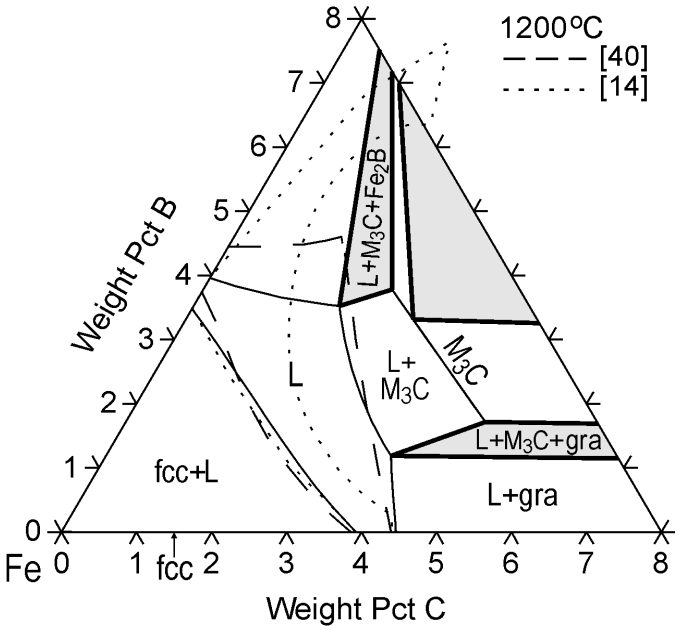

Fig. 12. Calculated isothermal section of the Fe-B-C system at 1200°C, together with the liquid phase region proposed by Schürmann and Li [40] (dashed line) and calculated by Ohtani et al. [14] (dotted line). The calculated three-phase triangles are shown in grey

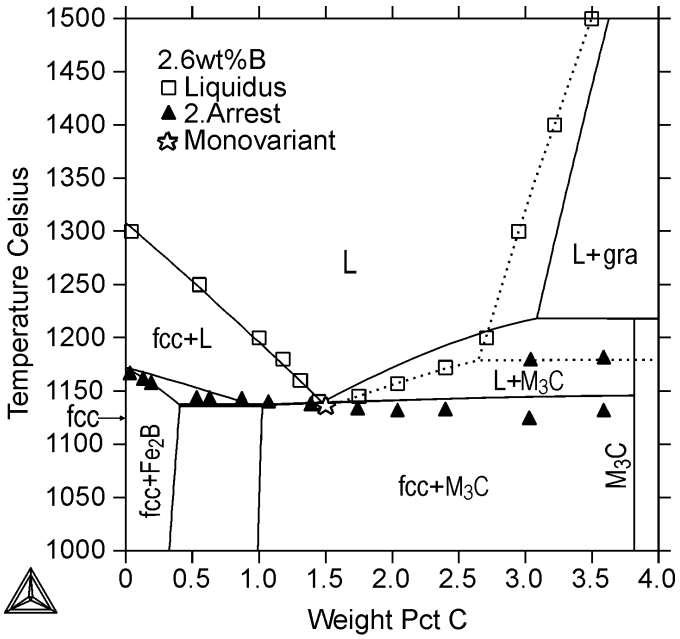

Fig. 11. Calculated vertical section of the Fe-B-C system at 2.6wt%B, together with experimental or estimated data points by Schürmann and Li [40]. The dotted lines show the phase regions of L + gra and L + M_3C as suggested by [40]

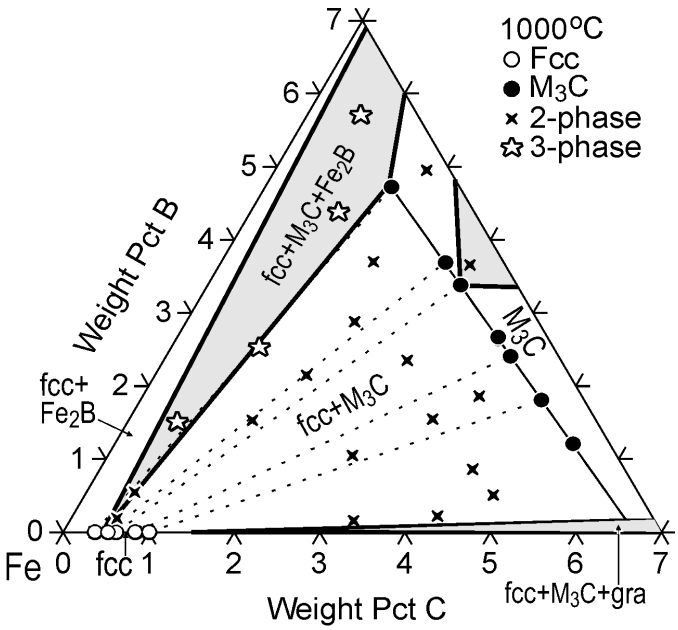

Fig. 13. Calculated isothermal section of the Fe-B-C system at 1000°C, together with experimental data points by Borlera and Pradelli [50], Hasebe and Nishizawa [51] and Lentz et al. [52]. The calculated three-phase triangles are shown in grey

and 700°C. In Figure 12, note the higher stability of the liquid phase at 1200°C by Schürmann and Li [40] than that obtained by the calculations by Ohtani et al. [14]. The present calculations agree better with the suggestions by [40], although at high B and low C compositions, the liquid phase stability remains much smaller, due to the binary Fe-B description fixed in an earlier study [1]. Concerning the isotherms where liquid is not present, note the absence of the graphite phase in Figure 18. It was suspended from the calculations because it was not detected in the measurements by Kaneko et al. [38] and Borlera and Pradelli [39]. Thus, Figure 18 represents a metastable diagram unlike the diagrams of Figures 12-17. Additionally, note the absence of the $M_{23}C_6$ phase at 1000°C (Figure 13) and its presence at 950°C (Figure 14). The precise high-temperature limit of the $M_{23}C_6$ decomposition was calculated to be 983°C, whereas according to measurements, $M_{23}C_6$ was observed to become unstable above

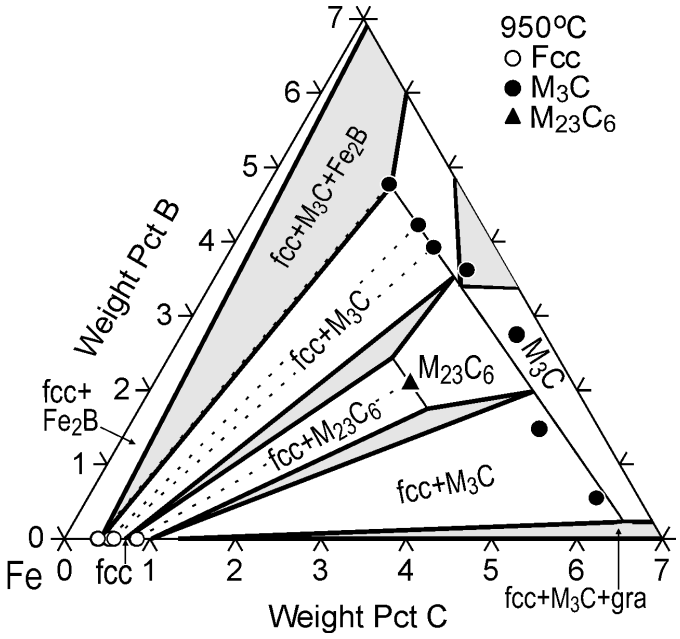

Fig. 14. Calculated isothermal section of the Fe-B-C system at 950°C, together with experimental data points by Kaneko et al. [38] and Hasebe and Nishizawa [51]. The calculated three-phase triangles are shown in grey

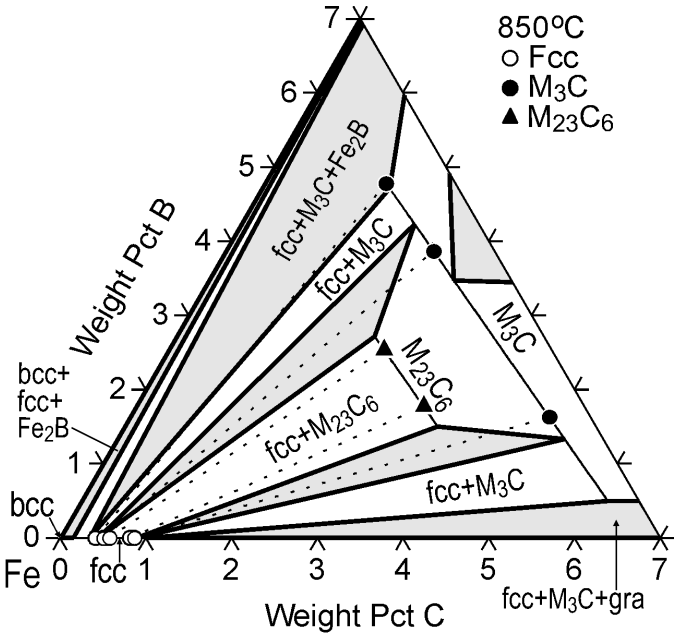

Fig. 16. Calculated isothermal section of the Fe-B-C system at 850°C, together with experimental data points by Hasebe and Nishizawa [51]. The calculated three-phase triangles are shown in grey

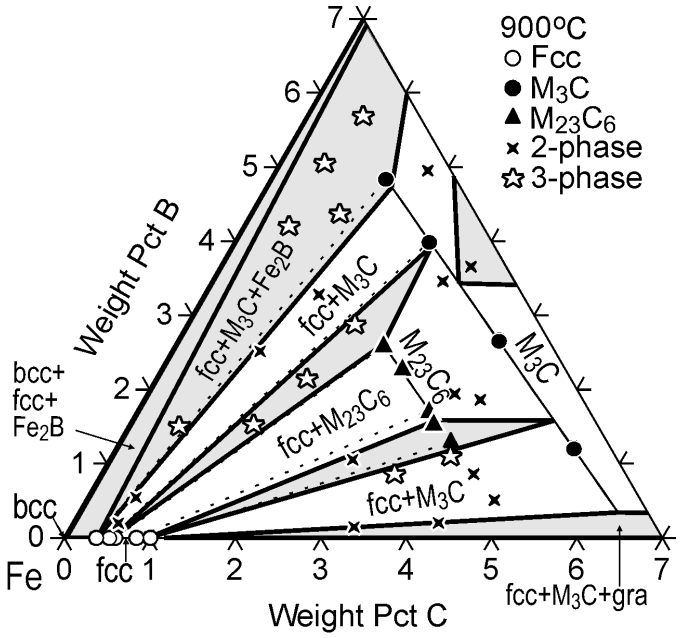

Fig. 15. Calculated isothermal section of the Fe-B-C system at 900°C, together with experimental data points by Borlera and Pradelli [50], Hasebe and Nishizawa [51] and Lentz et al. [52]. The calculated three-phase triangles are shown in grey

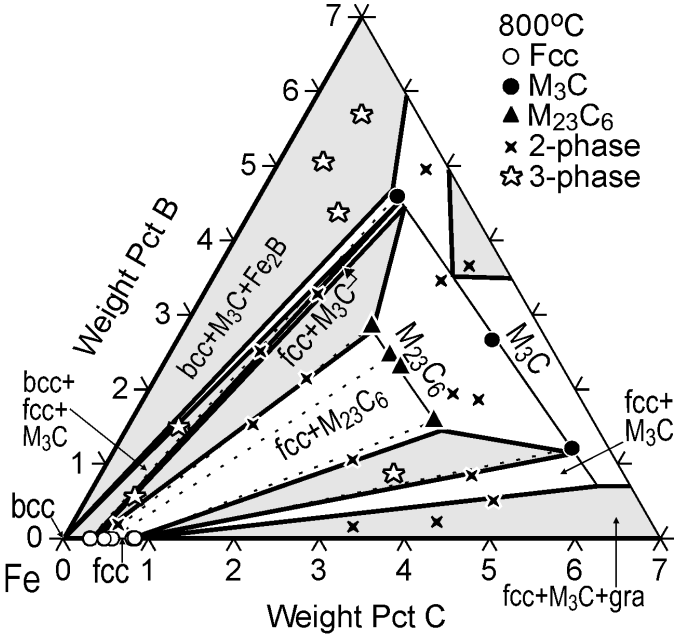

Fig. 17. Calculated isothermal section of the Fe-B-C system at 800°C, together with experimental data points by Borlera and Pradelli [50], Hasebe and Nishizawa [51] and Lentz et al. [52]. The calculated three-phase triangles are shown in grey

950°C [61] and at 966°C [50]. At low temperatures, the $M_{23}C_6$ phase disappears again from the structure. The measurements of Borlera and Pradelli [39] suggest the decomposition of $M_{23}C_6$ below 600°C, but when accepting the high stability of the phase at 700°C (Figure 18), it was not possible to get it to disappear in the calculations close to 600°C. By applying the simple M_3C and $M_{23}C_6$ phase descriptions given in Table 3, $M_{23}C_6$ disappears at a much lower temperature, i.e. 390°C. However, applying an alternative and more complex temperature function for parameter ${}^{\circ}G^{M_{23}C_6}_{Fe:Fe:B}$ given in Table 3, the temperature could be increased to 500°C, without causing any noticeable differences in the results of Figures 13 through 18. This is just to indicate that we still have some possibilities to affect the low-temperature phase equilibria of this system if new measurements become available. All in all,

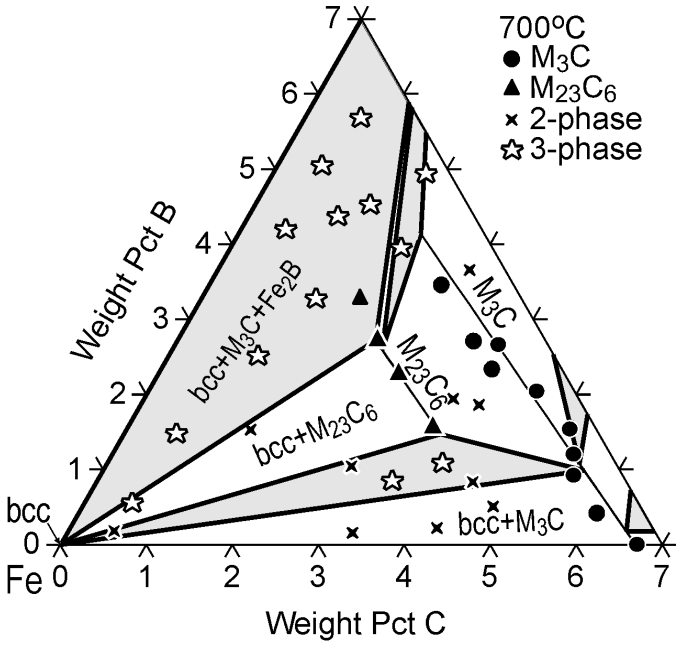

Fig. 18. Calculated isothermal section of the Fe-B-C system at 700°C, together with experimental data points by Kaneko et al. [38], Borlera and Pradelli [50] and Lentz et al. [52]. The calculated three-phase triangles are shown in grey. Graphite has been suspended from the calculations

the agreement between the calculations and measurements in all isotherms is quite good, taking into account the slight discrepancies between different measurements. As an example, compare the experimentally determined fcc + $M_{23}C_6$ regions at 900°C (Figure 15) and 850°C (Figure 16). At 900°C, the measurements by Kaneko et al. [38] show a more extensive homogeneity range for $M_{23}C_6$ than the calculations (see one black triangle of $M_{23}C_6$located in the fcc + $M_{23}C_6$ + M_3C region and the two star symbols of three-phase equilibria located in the fcc + M_3C region), whereas at 850°C, the homogeneity range by Hasebe and Nishizawa [51] is narrower than obtained by the calculations (see the measured fcc-M_3C tie lines going falsely through the two calculated three-phase triangles of fcc + $M_{23}C_6$ + M_3C). Consequently, we have a discrepancy between the measurements of [38,51], which cannot be satisfied by the calculations.

Finally, Figure 19 shows the calculated boron solubility in the fcc phase of the system. Increasing the C content promotes the formation of M_3C, which reduces the B solubility. The solubility is also reduced by a temperature drop from 1140°C to 1000°C. Shown also are the results of calculations treating carbon as a substitutional solution component [8] in the bcc and fcc phases. The corresponding data are given in Table 5. The deviation between these calculations is barely detectable indicating that the substitutional solution model works well for the bcc and fcc phases of the Fe-B-C system. Measured boron solubilities in the

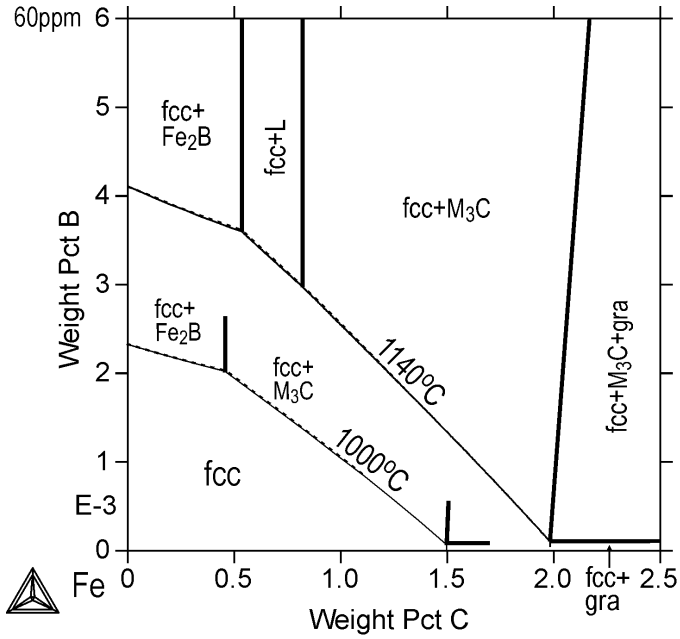

Fig. 19. Calculated solubility of B in the fcc phase of the Fe-B-C system at 1140°C and 1000°C. The lines refer to calculations treating carbon as an interstitial solution component and boron as a substitutional solution component in the bcc and fcc phases (Table 3) and broken lines refer to calculations treating both components as substitutional solution ones (Table 5)

TABLE 5

Thermodynamic descriptions of the substitutional solution bcc and fcc phases of the Fe-B-C system applied in the IAD database [8]. Thermodynamic data for pure Fe is taken from [53] and the parameter values except for T_C and β are in J/mol (see Table 3)

bcc (1 sublattice, sites: 1, constituents: B,C,Fe)	
${}^{o}G^{bcc}_{B} = {}^{o}G^{bet}_{B} + 43514 - 12.217T$	[54]
${}^{o}G^{bcc}_{C} = {}^{o}G^{gra}_{C} + 107350 + 35.764T$	[8]
$L^{bcc}_{B,Fe} = -50000 + 42T$	[1]
$L^{bcc}_{C,Fe} = -119.04T - 43.886T(x_C - x_{Fe}) - 7.858T(x_C - x_{Fe})^2$	[8]
$Tc^{bcc} = 1043(x_{Fe} + x_C) - 200x_{Fe}x_C$	[8]
$b^{bcc} = 2.22(x_{Fe} + x_C)$	[8]
fcc (1 sublattice, sites: 1, constituents: B,C,Fe)	
${}^{o}G^{fcc}_{B} = {}^{o}G^{bet}_{B} + 50208 - 13.478T$	[54]
${}^{o}G^{fcc}_{C} = {}^{o}G^{gra}_{C} + 155005 + 13.703T$	[8]
$L^{fcc}_{B,Fe} = -66000 + 50T$	[1]
$L^{fcc}_{C,Fe} = -162313 - 43.515T + (-60802 - 17.241T)(x_C - x_{Fe}) + (-10956 - 3.306T)(x_C - x_{Fe})^2$	[8]
$Tc^{fcc} = -201(x_{Fe} + x_C)$	[8]
$b^{fcc} = -2.1(x_{Fe} + x_C)$	[8]

fcc phase have been reported by Cameron [65], but unfortunately, this data is not available to the public. However, the effect of a C addition to reduce the boron solubility was stated.

Additional measurements for the solidus temperatures and the solid-state phase equilibria for three Fe-B-C alloys are available from Sudo et al. [66]. These data correlate somewhat moderately with the present calculations and those of the ThermoCalc software, which are close to each other. For the least alloyed steel of $Fe_{76}B_6C_{18}$ (at%), however, the measured solidus of 1125°C is reasonably close to the calculated value of 1149°C, and the measured structures of fcc + M_3C at 1000°C and $M_{23}C_6$ + M_3C at 800°C are identical to the calculated values. Measurements are available also for Fe-B-C alloys containing 30 to 60 at% B, by Homolová et al. [67], who determined three-phase triangles of Fe_2B + FeB + graphite, FeB + B_4C + graphite and FeB + B_4C + beta at 900°C and 600°C for eleven alloys. The current calculations agree well with these measurements. Nevertheless, this is only due to the simple treatment of the B_4C phase as a stoichiometric B_9C_2 phase (see Table 3). Instead, using the more eloquent B_4C descriptions by Kasper and Lukas [17], slight carbon solubility must be allowed in borides Fe_2B and FeB to satisfy the measurements, as demonstrated by Homolová et al. [67].

Due to the strong temperature and composition dependency introduced for the liquid state interaction parameter $L^{L}_{B,C,Fe}$, the present description is not recommended to be used at temperatures above 2700°C and at compositions above wt% C + wt% B > 15. At higher temperatures, the graphite solubility starts to behave in an unexpected manner, due to the increasing tendency of the liquid to form a miscibility gap. Before its formation, however, the bcc phase becomes falsely stable at 2969°C and with a composition of about 0.06 wt% B and 9.5 wt% C. Below 2700°C, however, the present liquid phase description works reasonably well.

4. Conclusions

A thermodynamic description was optimized for the ternary Fe-B-C system and its binary sub-system, B-C, applying experimental thermodynamic and phase equilibrium data from the literature. In these descriptions, 10 phases, i.e., liquid, bcc, fcc, beta-rhombo-B, graphite, M_3C (cementite), $M_{23}C_6$, Fe_2B, FeB and B_4C, were considered using the thermodynamic substitutional solution and sublattice models introduced earlier [18]. The descriptions of the beta-rhombo-B and B_4C phases of the B-C system were simplified from their more complex earlier versions [17]. This has only a marginal effect on the presented calculations. A good or reasonable correlation was obtained between the calculated and the experimental thermodynamic and phase equilibrium data, though only by introducing a relatively strong temperature and composition dependency for the liquid state interaction parameter $L^{L}_{B,C,Fe}$. Consequently, the current description works well only in the iron-rich corner of the system, within the composition range of wt% C + wt% B < 15 and at temperatures below 2700ºC.

The work continues the earlier started development for the Iron Alloy Database (IAD) [1-6,8] applied in the IDS software [9,10] to simulate the non-equilibrium solidification and solid-state phase transformations of steels. As that database treats boron and carbon as substitutional components, it was necessary to introduce two bcc and fcc phase descriptions, one for treating carbon as an interstitial solute (conventional treatment, Table 3) and one for treating it as a substitutional solute (IAD-treatment, Table 5). Due to the very low solubility of B in these phases, the results obtained by these two treatments are practically identical.

Acknowledgement

This study was executed within the framework of the Genome of Steel profiling project. The Academy of Finland (project 311934) and Walter Ahlström Foundation are acknowledged for funding this work.

REFERENCES

[1] J. Miettinen, G. Vassilev, Thermodynamic description of ternary Fe-B-X systems. Part 1: Fe-B-Cr, Arch. Metall. Mater. **59**, 601 (2014).

[2] J. Miettinen, G. Vassilev, Thermodynamic description of ternary Fe-B-X systems. Part 2: Fe-B-Ni, Arch. Metall. Mater. **59**, 609 (2014).

[3] J. Miettinen, K. Lilova, G. Vassilev, Thermodynamic description of ternary Fe-B-X systems. Part 3: Fe-B-Mn, Arch. Metall. Mater. **59**, 1481 (2014).

[4] J. Miettinen, V.-V. Visuri, T. Fabritius, N. Milcheva, G. Vassilev, Thermodynamic description of ternary Fe-B-X systems. Part 4: Fe-B-V, Arch. Metall. Mater. **64**, 451 (2019).

[5] J. Miettinen, V.-V. Visuri, T. Fabritius, N. Milcheva, G. Vassilev, Thermodynamic description of ternary Fe-B-X systems. Part 5: Fe-B-Si **64**, 1239 (2019).

[6] J. Miettinen, V.-V. Visuri, T. Fabritius, N. Milcheva, G. Vassilev, Thermodynamic description of ternary Fe-B-X systems. Part 6: Fe-B-Ti **64**, 1249 (2019).

[7] J.-O. Andersson, T. Helander, L. Höglund, P. Shi, B. Sundman, CALPHAD **26** 273 (2002).

[8] J. Miettinen, V.-V. Visuri, T. Fabritius, Thermodynamic description of the Fe-Al-Mn-Si-C system for modelling solidification of steels, Acta Universitatis Ouluensis C Technica **704**, Oulu University, Oulu, Finland (2019).

[9] J. Miettinen ,S. Louhenkilpi, H. Kytönen, J. Laine, Math. Comput. Simulat. **80**, 1536 (2010).

[10] J. Miettinen, S. Louhenkilpi, V.-V. Visuri, T. Fabritius, Advances in Modelling of Steel Solidification with IDS, IOP Conference Series: Materials Science and Engineering **529**, article 012063, 2019.

[11] S. Louhenkilpi, J. Miettinen, J. Laine, R. Vesanen, I. Rentola, J. Moilanen, V.-V. Visuri, E.-P. Heikkinen, A. Jokilaakso, Online Modelling of Heat Transfer, Solidification and Microstructure in

Continuous Casting of Steel, IOP Conference Series: Materials Science and Engineering **529**, article 012051, 2019.
[12] M. Hasebe, T. Nishizawa, J. Jpn. Inst. Metall. **38**, 46 (1974).
[13] T. Nishizawa, M. Hasebe, Tetsu-to-Hagane **67**, 2086 (1981).
[14] H. Ohtani, M. Hasebe, K. Ishida, T. Nishizawa, Trans. ISIJ **28**, 1043 (1988).
[15] B. Hallemans, P. Wollants, J.R. Roos, Z. Metallkd. **85**, 676 (1994). Aiemmin [54]
[16] P. Gustafson, Scand. J. Metall. **14**, 259 (1985).
[17] B. Kasper, H.L. Lukas, In: COST 507 – Thermochemical database for light metal alloys, **2**, I. Ansara, A.T. Dinsdale, M.H. Rand eds., European Communities, Belgium, pp.117–19 (1998).
[18] J.-O. Andersson, Metall. Trans. **19A**, 627 (1988).
[19] G. Hannesen, Z. Anorg. Chem. **89**, 257 (1914).
[20] K.I. Portnoi, M. Kh. Levinshkaya, V.M. Romashov, Sov. Powder Metall. Met. Ceram. **8**, 657 (1969).
[21] L.G. Voroshin, L.S. Lyakhovich, G.G. Panich, G.F. Protasevich, Met. Sci. Heat Treat. (USSR) **9**, 732 (1970).
[22] A. Brown, J.D. Garnish, R.W.K. Honeycombe, Metall. Sci. **8**, 317 (1974).
[23] T.B. Cameron, J.E. Morral, Metall. Trans. A **17A**, 1481 (1986).
[24] N.A. Vatolin, A.L. Zavialov, V.I. Zhuchkov, J. Less Common Met. **117**, 91 (1986)
[25] J. Chipman, R.M. Alfred, L.W. Gott, R.B. Small, D.M. Wilson, C.N. Tomson, D.L. Guernesy, J.C. Fulton, Trans. ASM **44**, 1215 (1952).
[26] R.P. Smith, L.S. Darken, Trans. Met. Soc. AIME **215**, 727 (1959).
[27] R.A. Buckley, W. Hume-Rothery, J. Iron Steel Inst. **196**, 403 (1960).
[28] M. Benz, J. Elliott, Trans. AIME **221**, 323 (1961).
[29] F. Neumann, H. Schenck, Giesserei Techn.-Wiss. Beih. **14**, 21 (1962).
[30] T. Wada, H. Wada, J.F. Elliott, J. Chipman, Metall. Trans. **2**, 2199 (1971).
[31] B. Chicco, W.R. Thorpe, Metall. Trans. A, **14A**, 312 (1983).
[32] M. Hasebe, H. Ohtani, T. Nishizawa, Met. Trans. A, **16A**, 913 (1985).
[33] R.P. Elliott, The Boron-Carbon system, Final Technical Report, ARF-2000-12 for U.S. Atomic Energy Comission, Contract No. AT(11-1)-578, 50 (1961).
[34] F. Thevenot, J. European Ceramic Society **6**, 205 (1990).
[35] C.E. Lowell, J. Am. Ceram. Soc. **50**, 142 (1967).
[36] V. Raghavan, Phase Diagrams of Ternary Iron Alloys – Part 6A, Indian Institute of Metals, Calcutta, India, pp. 287-96 (1992).
[37] P. Rogl, Materials Science International Team, MSIT®, Boron-Carbon-Iron. G. Effenberg, I. Svitlana eds., Springer Materials – The Landolt-Börnstein Database, Springer-Verlag Berlin Heidelberg (2008).
[38] H. Kaneko, T. Nishizawa, A. Chiba, Nippon Kinzoku Gakkai-Si **30**, 263 (1966).
[39] M.L. Borlera, G. Pradelli, Metall. Ital. **60**, 140 (1968).
[40] E. Schürmann, S.-X. Li, Giessereiforschung **37**, 121 (1985).
[41] T. Miki, K. Tsujita, S. Ban-Ya, M. Hino, CALPHAD **30**, 449 (2006).
[42] B.P. Burlyev, Izv. Vysh. Uchebn. Zaved. Cern. Metall. **6**, 5 (1965).
[43] D.L. Ball, Trans. Met. Soc AIME **239**, 31 (1967).
[44] H. Schenck, M.G. Frohberg, E. Steinmetz, B. Rutenberg, Arch. Eisenhüttenwes. **33**, 223 (1962).
[45] S. Sunkar, K. Morita, AIST Transactions **6**, 164 (2009).
[46] R. Yu, S. Liu, C. Ji, Iron and Steel (China) **22**, 8 (1987).
[47] X. Huang, W.G. Ischak, H. Fukuyama, T. Fujisawa, C. Yamauchi, Tetsu-to-Hagane **81**, 1049 (1995).
[48] R. Vogel, G. Tammann, Z. Anorg. Allgem. Chemie **123**, 225 (1922).
[49] J. Lentz, A. Röttger, W. Theisen, Acta Mater. **99**, 119 (2015).
[50] M. Borlera, G. Pradelli, Metall. Ital. **59**, 907 (1967).
[51] M. Hasebe, T. Nishizawa, Nihon Ginzoku Gakkaishi **38**, 46 (1974).
[52] J. Lentz, A. Röttger, W. Theisen, Acta Mater. **119**, 80 (2016).
[53] A. T. Dinsdale, SGTE unary database, version 4.4; www.sgte.org A.T. Dinsdale, CALPHAD **15**, 317 (1991).
[54] I. Ansara, A.T. Dinsdale, M.H. Rand, COST 507 – Thermochemical database for light metal alloys, Volume 2, European Communities, Belgium (1998).
[55] D. Djurovic, B. Hallstedt, J. von Appen, R. Dronskowski, CALPHAD **35**, 479 (2011).
[56] N. Saunders, A. P. Miodownik, CALPHAD: A Comprehensive Guide, Pergamon Press, Oxford, United Kingdom (1998).
[57] B. Hallstedt, D. Djurovic, J. von Appen, R. Dronskowski, A. Dick, F. Körmann, T. Hickel, J. Neugebauer, CALPHAD **34**, 129 (2010)
[58] M. Yukinobu, O. Ogawa, S. Goto, Metall. Trans. B **20B**, 705 (1989).
[59] A.I. Zaitsev, N.E. Zaitseva, A.A. Kodentsov, Metall. Mater. Trans. B **34B**, 887 (2003).
[60] M.E. Nicholson, Trans. Met. Soc. AIME **209**, 1 (1957).
[61] O.I. Fomichev, V.F. Katkov, A.K. Kushnereva, Inorg. Mater. **12**, 111 (1976).
[62] O.I. Fomichev, V.F. Katkov, A.K. Kushnereva, Russ. J. Phys. Chem. **52**, 1294 (1978)
[63] H.H. Stadelmaier, R.A. Gregg, Metall (Berlin), **17** (1963) 412-14.
[64] V.T. Witusiewicz, J. Alloys Compounds **203**, 103 (1994).
[65] T.B. Cameron, Thesis "The Influence of Carbon on Boron Solubility in Austenite", Diss. Abstr. Int. **45**, 142 (1985).
[66] A. Sudo, T. Nishi, N. Shirasu, M. Takano, M. Kurata, J. Nucl. Sci. Tech. **52**, 1308 (2015).
[67] V. Homolová, L. Čiripová, A. Výrostková, J. Phase Equilibria and Diffusion **36**, 599 (2015).